PHYSICAL REVIEW C VOLUME 48, NUMBER 4 OCTOBER 1993

Photon-hadron interactions in relativistic heavy ion collisions

N. Baron and G. Baur
Institut für Kernphysik (Theorie), Forschungszentrum Jülich, W-5170 Jülich, Germany
(Received 17 May 1993)

High-energy photon-hadron interactions in relativistic heavy ion collisions are studied in the impulse approximation. This leads to an explicit treatment of the spatial distribution of the constituents in the volume of the nucleus struck by the equivalent photon. Relevant changes in the high-energy tail of the equivalent photon spectrum compared to the conventional method are obtained. Total fragmentation cross sections due to photon-hadron interactions which contribute to the luminosity decrease at colliders like the Brookhaven Relativistic Heavy Ion Collider or the CERN Large Hadron Collider (heavy ions) are also studied. As an important application we study the γg fusion into quark-antiquark pairs. This gives a handle to determine the gluon distribution function of nucleons inside the nucleus.

PACS number(s): 25.75.+r

I. INTRODUCTION

Heavy ions at ultrarelativistic velocities are an intense source of quasireal photons. Relativistic heavy ion colliders are planned in Brookhaven [Relativistic Heavy Ion Collider (RHIC)] and at CERN [Large Hadron Collider (LHC)] with center of mass (c.m.) energies of 100 and 3400 GeV/nucleon, respectively. Because of the coherence factor Z^2 in the spectrum, an intense flux of high-energy photons accompanies the heavy ions. Equivalent photon energies in the collider frame up to 3 and 100 GeV for RHIC and LHC, respectively, are obtained.

In peripheral collisions (with impact parameters $b \geq R_1 + R_2$) with no strong interactions between the colliding nuclei, reactions are purely due to electromagnetic interactions of the equivalent photons. In close collisions, where very high equivalent photon energies are available, these photons may directly interact with the constituents of the struck nucleus, i.e., nucleons, quarks, gluons, etc. For high equivalent photon energies it is a fairly good assumption to work in the impulse approximation (see, for example, Ref. [1]). The conventional equivalent photon approach for the calculation of corresponding cross sections in peripheral collisions (see, e.g., [2]) works with an average over the volume of the nucleus; i.e., the impact parameter b is simply the distance between the c.m.'s of the colliding nuclei in the transversal plane. Because of the strong b dependence of the equivalent photon spectrum for close collisions, an appropriate formulation of the interaction with the constituents of the nuclei has to consider the impact parameter of the single constituent. A modified equivalent photon spectrum in the impulse approximation considering this effect was first proposed in Ref. [3].

It is the purpose of this paper to study the interaction of high-energy equivalent photons with the constituents of the nuclei in relativistic heavy ion collisions. Special care is taken of the modified equivalent photon method in comparison to the conventional one. In Sec. II we present the improved formulation of the impact parameter dependent equivalent photon spectrum in the impulse approximation in detail. We explicitly derive the spectrum valid for peripheral collisions and give analytic formulas in a sharp cutoff approximation.

Numerical results are given in Sec. III. An explicit comparison of the improved equivalent photon spectrum to the conventional one is given in Sec. III A. An interesting application is the contribution to the luminosity decrease in relativistic heavy ion colliders [4,5]. At relativistic heavy ion colliders one has the opportunity to study the photonuclear cross sections at very high energies and effects due to the modified equivalent spectra may be important. This is studied in detail in Sec. III B.

The gluon distribution function in nuclei may be determined via the investigation of the $\gamma g \rightarrow q\bar{q}$ subprocess in relativistic heavy ion collisions as proposed in Ref. [6]. This process is determined theoretically by folding the equivalent photon spectrum and the gluon distribution function. Therefore it is essential to use an accurate equivalent photon spectrum at high energies as a theoretical input. In Sec. IV we study the production of $c\bar{c}$ via γg fusion in relativistic heavy ion collisions in view of a possible determination of the gluon distribution function.

Our conclusions are given in Sec. V.

II. THEORY: GEOMETRICAL MODIFICATIONS OF THE EQUIVALENT PHOTON SPECTRUM

In the equivalent photon approximation the cross section for a photonuclear reaction in a relativistic heavy ion collision is given by

$$\frac{d\sigma}{d\omega} = \frac{n(\omega)}{\omega} \sigma_{\gamma A}(\omega) , \tag{2.1}$$

where $\sigma_{\gamma A}$ is the on-shell elementary photonuclear cross section. The equivalent photon spectrum $n(\omega)$ in Eq. (2.1) is conventionally obtained via

$$n(\omega) = \int_{b \geq 2R} d^2b \, N(\omega, b) , \tag{2.2}$$

where the peripheral collision of two nuclei of the same

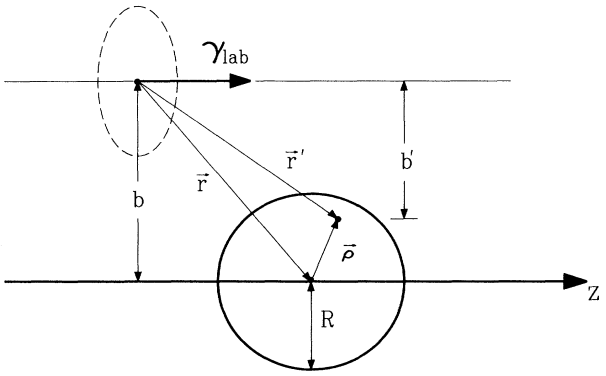

FIG. 1. Schematical picture of the peripheral collision of two nuclei in the fixed target system. The conventional equivalent photon method uses the impact parameter b defined through the distance of the c.m.'s of the colliding nuclei. The improved method takes into account the finite spatial distribution of scatterers in the nuclei leading to the explicit occurrence of distances $b' < b$.

mass number ($R_1+R_2=2R$) is assumed. $N(\omega,b)$ is given in Refs. [7,2,8]. The integration in Eq. (2.2) explicitly reflects the condition of peripheral collisions; i.e., there is no overlap between the two nuclei (for R the nuclear charge radius is conventionally used).

In the impulse approximation the photonuclear cross section $\sigma_{\gamma A}$ is interpreted as the superposition of all photon-constituent interactions. Therefore Eq. (2.2) implicitly contains an averaging over the distribution of constituents in the volume of the struck nucleus: For the impact parameter in Eq. (2.2) the distance between the c.m.'s of the colliding nuclei is used. For large distances, i.e., $b \gg 2R$, this is a good approximation, though, in the case of close collisions, the difference of this effective impact parameter to the one considering the spatial distribution of the constituents in the transversal plane becomes important. In fact, for high-energy equivalent photons the scaling variable $x=\omega b/\gamma v$ which determines the exponential decrease of the spectrum for $x \geq 1$ is sensitive on the value of b. In the conventional picture the minimum impact parameter is given by $2R$, leading to the maximum equivalent photon energy available in peripheral collisions:

$$\omega_{\max}=\frac{\gamma\hbar c}{2R} . \tag{2.3}$$

The consideration of a finite spatial distribution of the constituents allows for even smaller impact parameters b' in certain volume elements of the struck nucleus. This is illustrated schematically in Fig. 1. This consequently leads to a different maximum equivalent photon energy for these constituents. The minimum impact parameter b' is given by $b'=R$.

A. Theoretical formulation and discussion

To treat the impact parameter dependence of the equivalent photon spectrum properly, we start with the semiclassical excitation amplitude for the interaction of photons with matter:

$$a_{fi}=\frac{1}{i}\int dt\, e^{i\omega t}\langle f|V[\mathbf{r}(t)]|i\rangle , \tag{2.4}$$

where the interaction potential is given by

$$V[\mathbf{r}(t)]=\int d^3r\, A_\mu(\mathbf{r},t)j^\mu(\mathbf{r}) . \tag{2.5}$$

Assuming that the nucleus with charge Ze moves on a straight line with impact parameter b and constant velocity leads to a vector potential (see, e.g., [7]) of the form

$$A_\mu(\mathbf{r},t)=\Phi(\mathbf{r},t)v_\mu = v_\mu\frac{Ze\gamma}{2\pi^2}\int d^3p\frac{e^{i\mathbf{p}\cdot(\mathbf{R}-\mathbf{R}')}}{p^2} , \tag{2.6}$$

where $v_\mu=(1,0,0,v)$. In Eq. (2.6) we introduced $\mathbf{R}=(x,y,\gamma z)$ and $\mathbf{R}'=(\mathbf{b},\gamma vt)$.

In the impulse approximation we assume that the coupling of the equivalent photon to the constituent of the struck nucleus, say, a nucleon, is the same as if it were free. For the energy scale under consideration, i.e., high equivalent photon energies due to close collisions, this is a good approximation (see, e.g., Ref. [1]). The Fermi momentum of the nucleons inside the nucleus is neglected; the nucleons may be seen as fixed relative to the c.m. of the nucleus (frozen nucleus approximation). Therefore, the current density in Eq. (2.5) is simply the internal nucleon current density.

To take explicitly reference to the position of the nucleon inside the nucleus we simply introduce c.m. coordinates of the nucleon in Eqs. (2.5) and (2.6). The interaction potential is then given by

$$V[\mathbf{r}(t)]=\frac{Ze\gamma}{2\pi^2}\int d^3p\int d^3r\frac{e^{i\mathbf{p}\cdot(\mathbf{R}+\boldsymbol{\rho}-\mathbf{R}')}}{p^2}v_\mu j_N^\mu(\mathbf{r}) , \tag{2.7}$$

where $\boldsymbol{\rho}=(\boldsymbol{\rho}_\perp,\gamma\rho_z)$ is the position of the nucleon relative to the c.m. of the nucleus.

For the wave functions $|i\rangle,|f\rangle$ we take

$$|i\rangle=|N_0\rangle|\phi_0\rangle , \quad |f\rangle=|N_f\rangle|\phi_f\rangle . \tag{2.8}$$

In Eq. (2.8), $|N\rangle$ is the internal nucleon wave function and $|\phi\rangle$ is the wave function (for example, the shell-model wave function) for the center of mass of the nucleon.

Inserting Eq. (2.7) into Eq. (2.4) and writing more explicitly

$$a_{fi}=\frac{1}{i}\frac{Ze\gamma}{2\pi^2}\langle\phi_f|\langle N_f|\int d^3p\int d^3r\int dt\, e^{i(\omega-p_z\gamma v)t}\frac{e^{i\mathbf{p}\cdot(\mathbf{R}+\boldsymbol{\rho})}}{p^2}e^{-i\mathbf{p}_\perp\cdot\mathbf{b}}v_\mu j_N^\mu(\mathbf{r})|N_0\rangle|\phi_0\rangle , \tag{2.9}$$

we can carry out integration over t directly. The resulting δ function can be used to carry out the integration over p_z.

We finally find, for the amplitude Eq. (2.9),

$$a_{fi}=\frac{1}{i}\frac{Ze}{\pi v}\langle\phi_f|\int d^2p_\perp\frac{e^{i\mathbf{p}_\perp\cdot(\mathbf{b}-\boldsymbol{\rho}_\perp)}}{p_\perp^2+(\omega/\gamma v)^2}e^{i\omega\rho_z/v}|\phi_0\rangle\langle N_f|\int d^3r\,e^{i\mathbf{p}'\cdot\mathbf{r}}v_\mu j_N^\mu(\mathbf{r})|N_0\rangle\ . \tag{2.10}$$

The momentum $\mathbf{p}'$ in Eq. (2.10) is given by $\mathbf{p}'=(\mathbf{p}_\perp,\omega/v)$.

The nucleon matrix element in Eq. (2.10) can be rewritten with the help of the continuity equation (see, e.g., Refs. [9,2]). In the ultrarelativistic limit we have

$$\langle N_f|\int d^3r\,e^{i\mathbf{p}'\cdot\mathbf{r}}v_\mu j_N^\mu(\mathbf{r})|N_0\rangle=\langle N_f|\int d^3r\,e^{i\mathbf{p}'\cdot\mathbf{r}}\frac{\mathbf{p}_\perp\cdot\mathbf{j}_N^\perp(\mathbf{r})}{\omega}|N_0\rangle\ . \tag{2.11}$$

Inserting in Eq. (2.10) gives

$$a_{fi}=\frac{1}{i}\frac{Ze}{\pi v}\frac{1}{\omega}\langle\phi_f|\int d^2p_\perp\frac{\mathbf{p}_\perp\cdot e^{i\mathbf{p}_\perp\cdot(\mathbf{b}-\boldsymbol{\rho}_\perp)}}{p_\perp^2+(\omega/\gamma v)^2}e^{i\omega\rho_z/v}|\phi_0\rangle\langle N_f|\int d^3r\,e^{i\mathbf{p}'\cdot\mathbf{r}}\mathbf{j}_N^\perp(\mathbf{r})|N_0\rangle\ . \tag{2.12}$$

The probability of the inclusive process is given by summing over ϕ_f,

$$\frac{dP_{\gamma N}}{d\omega}=\sum_{\phi_f}|a_{fi}|^2\ . \tag{2.13}$$

Explicitly, this leads to

$$\frac{dP_{\gamma N}}{d\omega}=\frac{Z^2\alpha}{\pi^2v^2}\frac{1}{\omega}\sum_{\phi_f}\langle\phi_0|\int d^2p_\perp\frac{\mathbf{p}_\perp\cdot e^{i\mathbf{p}_\perp\cdot(\mathbf{b}-\boldsymbol{\rho}_\perp)}}{p_\perp^2+(\omega/\gamma v)^2}e^{-i\omega\rho_z/v}|\phi_f\rangle\langle\phi_f|\int d^2p_\perp\frac{\mathbf{p}_\perp\cdot e^{-i\mathbf{p}_\perp\cdot(\mathbf{b}-\boldsymbol{\rho}_\perp)}}{p_\perp^2+(\omega/\gamma v)^2}e^{i\omega\rho_z/v}|\phi_0\rangle$$
$$\times\frac{1}{\omega}\left|\langle N_f|\int d^3r\,e^{i\mathbf{p}'\cdot\mathbf{r}}\mathbf{j}_N^\perp(\mathbf{r})|N_0\rangle\right|^2\ . \tag{2.14}$$

The length scale connected with the nucleon matrix element $\langle N_f|\cdots|N_0\rangle$ is much smaller than the one connected with the nuclear matrix element $\langle\phi_f|\cdots|\phi_0\rangle$. Therefore, in the equivalent photon approximation, the transverse momentum dependence in the exponential of the matrix element $\langle N_f|\cdots|N_0\rangle$ can be neglected. In this case, the last factor on the right-hand side of Eq. (2.14) is straightforwardly connected to the total elementary photonuclear cross section $\sigma_{\gamma N}(\omega)$. The wave functions $|\phi\rangle$ form a complete set and we may apply closure over the final states $|\phi_f\rangle$. We finally find

$$\frac{dP_{\gamma N}}{d\omega}=\frac{Z^2\alpha}{\pi^2v^2}\langle\phi_0|\left|\int d^2p_\perp\frac{\mathbf{p}_\perp e^{-i\mathbf{p}_\perp\cdot(\mathbf{b}-\boldsymbol{\rho}_\perp)}}{p_\perp^2+(\omega/\gamma v)^2}\right|^2|\phi_0\rangle\frac{\sigma_{\gamma N}(\omega)}{\omega}\ . \tag{2.15}$$

The remaining integral in Eq. (2.15) can directly be related to the impact parameter dependent equivalent photon spectrum deduced in Refs. [8,10]. Introducing explicit coordinate space representations we rewrite Eq. (2.15):

$$\frac{dP_{\gamma N}}{d\omega}=\int d^3\rho|\phi_0(\boldsymbol{\rho})|^2N(\omega,|\mathbf{b}-\boldsymbol{\rho}_\perp|)\frac{\sigma_{\gamma N}(\omega)}{\omega}\ . \tag{2.16}$$

In Eq. (2.16), $|\phi_0|^2$ is the probability density of finding a nucleon at $\boldsymbol{\rho}$ in the target nucleus.

Comparison with Eq. (2.1) and introducing a short notation for the probability density (renaming variables) leads to a geometrically modified equivalent photon spectrum:

$$N_\rho(\omega,b)=\int d^3r\,\rho(\mathbf{r})N(\omega,|\mathbf{b}-\mathbf{r}_\perp|)\ , \tag{2.17}$$

where $\rho(\mathbf{r})$ denotes the probability density of finding a nucleon at $\mathbf{r}$ in the target nucleus.

By integrating Eq. (2.17) over the impact parameter we can define a geometrically modified integrated equivalent photon spectrum $n_\rho(\omega)$.

We want to point out that in the equivalent photon spectrum Eq. (2.17) properties of the target nucleus as well as of the projectile nucleus are contained. On the right-hand side $\rho(\mathbf{r})$ is the probability distribution of the nucleons in the target nucleus, while $N(\omega,|\mathbf{b}-\mathbf{r}|)$ in principle contains the charge form factor of the projectile. This is in contrast to the conventional method, where only the properties of the nucleus creating the equivalent photon spectrum enter.

We also want to stress that Eq. (2.17) is only valid for peripheral collisions. This reads $b\geq R_T+R_P$ and accordingly $b'=|\mathbf{b}-\mathbf{r}|>R_P$, where R_T and R_P are the radii of the target and projectile, respectively.

Furthermore, it is straightforward to replace $\sigma_{\gamma N}$ in Eq. (2.16) by any elementary cross section for a γ-constituent reaction; i.e., the calculation is independent of the special nuclear constituent under consideration. Accordingly, the related probability density has to be used.

B. Analytical reductions

In the case of a heavy nucleus such as ^{208}Pb the probability density of finding a nucleon inside the nucleus can be approximated by

$$\rho(\mathbf{r})=\begin{cases}\dfrac{1}{4\pi R^3/3}\ , & |\mathbf{r}|\le R\ ,\\ 0\ , & |\mathbf{r}|>R\ ,\end{cases} \tag{2.18}$$

where R denotes the charge radius of the nucleus. Since the impact parameter dependent modified equivalent photon spectrum in Eq. (2.17) only depends on the transversal components of $\mathbf{r}$, integration over the third component using Eq. (2.18) for the target nucleus can be carried out. We get

$$N_\rho(\omega,b)=\int d^2r_\perp \frac{2\sqrt{R^2-r_\perp^2}}{4\pi R^3/3} N(\omega,|\mathbf{b}-\mathbf{r}_\perp|)\ . \tag{2.19}$$

Using Eq. (2.18) for the target nucleus, we have to use accordingly a form factor of a spherical charge distribution for the projectile. It is well known that the conventional equivalent photon spectrum of a homogeneously charged sphere coincides with the one of a point particle of the same charge with a lower cutoff at the radius as long as peripheral collisions are concerned. Therefore we use

$$N(\omega,b')=\frac{Z^2\alpha}{\pi^2}\frac{1}{b'^2}\left[x^2K_1^2(x)+\frac{x^2}{\gamma^2}K_0^2(x)\right]\ , \tag{2.20}$$

where $b'=|\mathbf{b}-\mathbf{r}|>R$ and $x=\omega b'/\gamma v$.

In a sharp cutoff approximation we have

$$\left[x^2K_1^2(x)+\frac{x^2}{\gamma^2}K_0^2(x)\right]=\begin{cases}1\ , & 0\le x\le 1\ ,\\ 0\ , & x>1\ .\end{cases} \tag{2.21}$$

The condition for x in Eq. (2.21) has to be interpreted as a condition for b'. The spectrum in this approximation then reads

$$N^{\rm app}(\omega,b')=\begin{cases}\dfrac{Z^2\alpha}{\pi^2}\dfrac{1}{b'^2}\ , & R_P\le b'\le\gamma/\omega\ ,\\ 0\ , & b'>\gamma/\omega\ ,\end{cases} \tag{2.22}$$

where $b'=\sqrt{b^2+r^2-2br\cos\varphi_r}$. In Eq. (2.22) we set without loss of generality $\mathbf{b}=(b,0)$. In this case we can solve Eq. (2.19) analytically.

For A-A collisions, i.e., $R_T=R_P=R$, the geometrically modified equivalent photon spectrum Eq. (2.19) is given by

$$N_\rho^{\rm app}(\omega,b)=\frac{Z^2\alpha}{\pi^2}\frac{2}{4\pi R^3/3}\int_0^R r\,dr\sqrt{R^2-r^2}\int_0^{2\pi}d\varphi\frac{1}{b^2+r^2-2br\cos\varphi}\ . \tag{2.23}$$

The integrations can be done analytically (see, e.g., Ref. [11]) leading to an approximated spectrum of the form

$$N_\rho^{\rm app}(\omega,b)=\frac{Z^2\alpha}{\pi^2}\frac{4\pi R}{4\pi R^3/3}\left[1-\frac{\sqrt{b^2-R^2}}{R}\arctan\left[\frac{R}{\sqrt{b^2-R^2}}\right]\right]\ ,\quad \text{for } b>2R\ ,\ b+R<\gamma/\omega\ . \tag{2.24}$$

The approximation Eq. (2.24) is expected to be very good in the case

$$\frac{\omega(b+R)}{\gamma\hbar c}\ll 1\ . \tag{2.25}$$

For large impact parameters b, Eq. (2.24) can be expanded in terms of $z=R/b$, leading to

$$N_\rho^{\rm app}(\omega,b)=\frac{Z^2\alpha}{\pi^2}\frac{1}{b^2}\left[1+\frac{2}{5}z^2\pm\cdots\right]\ . \tag{2.26}$$

In principle, it is possible to integrate Eq. (2.24) analytically over the impact parameter. This leads mainly to the integral $\int(du/u^4)\arctan u$, which results in a very involved expression.

III. NUMERICAL RESULTS

In Sec. II we modified the usual equivalent photon spectrum by taking into account the finite spatial distribution of constituents in the nucleus struck by the equivalent photon. First, we compare the equivalent photon spectra $N(\omega,b)$, $N_\rho(\omega,b)$, and $N_\rho^{\rm app}(\omega,b)$ as well as the integrated spectra $n(\omega)$ and $n_\rho(\omega)$. This stresses the necessity of the geometrically improved equivalent photon spectrum for calculations of high-energy equivalent photon interactions in relativistic heavy ion collisions.

In the second part we apply Eq. (2.1) to the calculation of the total fragmentation cross section relativistic heavy ion colliders.

A. Comparison of the equivalent photon spectra

In the following we compare the different equivalent photon spectra. For the geometrically improved spectrum we use Eq. (2.19) with Eq. (2.20) and integrate numerically as well as the analytical approximation Eq. (2.24). The spectrum used so far is given by Eq. (2.20) at $b'=b$.

In the formulation of the equivalent photon spectrum Eq. (2.19) the laboratory frame probability density of the target enters. The relevant transformations to the collider (c.m.) system are given by

$$\gamma_{\rm lab}=2\gamma_{\rm coll}^2-1\ ,\quad \omega_{\rm lab}=\gamma_{\rm coll}(1+v)\omega_{\rm coll}\ . \tag{3.1}$$

From Eq. (3.1) we find, in the ultrarelativistic limit,

$$\frac{\omega_{\rm lab}}{\gamma_{\rm lab}}\simeq\frac{\omega_{\rm coll}}{\gamma_{\rm coll}}\ . \tag{3.2}$$

Since it is well known that the equivalent photon spectrum scales with ω/γ, we characterize the spectra by their scaling variable $\tilde{x}=\omega/\gamma$ in the following.

In Figs. 2 and 3 the impact parameter dependent equivalent photon spectrum as a function of the impact parameter for fixed values of $\tilde{x}=\omega/\gamma$ is shown. The spectra are calculated for ^{208}Pb-^{208}Pb collisions where $R=7$ fm is assumed.

In Fig. 2 we fixed $\tilde{x}=\frac{1}{3400}$ GeV, i.e., $\omega=1$ GeV for LHC or $\omega=29$ MeV for RHIC conditions, respectively. The restriction to peripheral collisions leads to a lower limit of the spectra of $b_{\rm min}=14$ fm. The solid line corresponds to $N_\rho(\omega,b)$ via Eqs. (2.19) and (2.20), while the dashed line corresponds to the spectrum $N(\omega,b)$. For large impact parameters the two spectra coincide. This property can be seen directly from Eq. (2.20); for $b\gg R$ we have $b'\simeq b$ and the integration in Eq. (2.19) is trivial, leading to $N_\rho(\omega,b)\simeq N(\omega,b)$. For close collisions the spectrum $N_\rho(\omega,b)$ is harder than the other one. This tendency may also be understood from the basic idea of the modification: For close collisions there are relevant contributions to the spectrum from $R\le b'\le 2R$ which do not occur in the conventional approach; the averaging process over the target volume is no longer accurate.

In Fig. 3 the same quantity as in Fig. 2 is shown at $\tilde{x}=\omega/\gamma=\frac{3000}{100}$ MeV; the labeling of the curves is also the same. The value of $\tilde{x}$ in Fig. 3 is large enough that the spectra are reduced by one order of magnitude for small impact parameters in comparison to Fig. 2. In this case the contributions from $R\le b'\le 2R$ lead to much larger differences (more than a factor of 2) between the spectra.

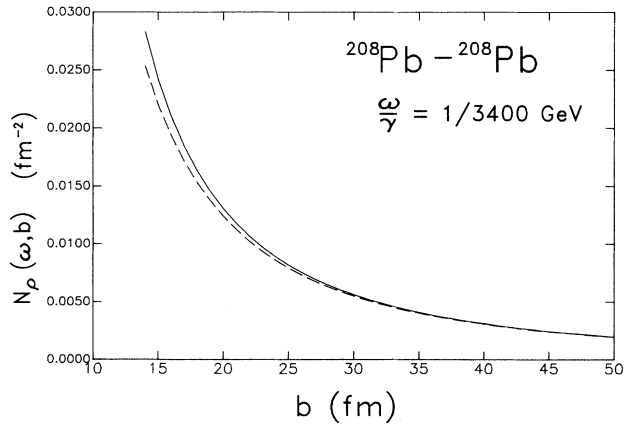

FIG. 2. Impact parameter dependent equivalent photon spectrum as a function of the impact parameter b for fixed values of the scaling variable $\tilde{x}=\omega/\gamma=\frac{1}{3400}$ GeV. The dashed line corresponds to the usual $N(\omega,b)$, while the solid line corresponds to $N_\rho(\omega,b)$. The spectra are calculated for the ^{208}Pb-^{208}Pb system where $R=7$ fm is assumed.

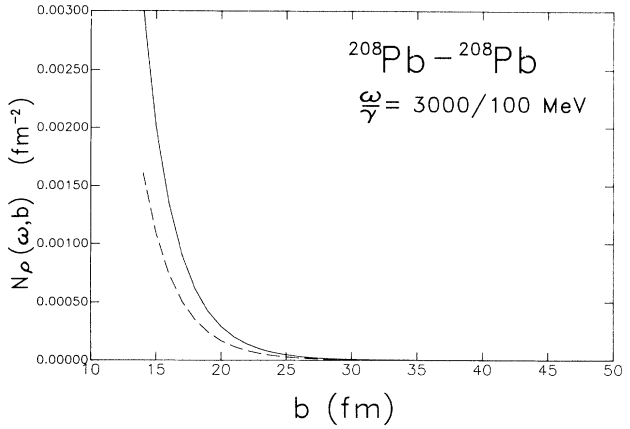

FIG. 3. Same quantity as in Fig. 2 for $\tilde{x}=\frac{3000}{100}$ MeV.

As shown in Figs. 2 and 3 the absolute deviation of $N_\rho(\omega,b)$ from $N(\omega,b)$ for close collisions depends on the value of the scaling variable $\tilde{x}$. To study the net difference between the spectra the impact parameter integrated spectra have to be studied as a function of ω or ω/γ. This is done in Fig. 4 where the impact parameter integrated equivalent photon spectrum as a function of $\tilde{x}=\omega/\gamma$ is shown for the ^{208}Pb-^{208}Pb system. The solid line corresponds to the spectrum $n_\rho(\omega)$ calculated from Eq. (2.19), while the dashed line shows the conventional result $n(\omega)$ (see, e.g., Ref. [2]). The curves are universal in the sense that they may be applied to RHIC and LHC conditions by considering the appropriate Lorentz factor. For small $\tilde{x}$ the two integrated spectra do not differ significantly, while for larger $\tilde{x}$ the decrease of $n(\omega)$ is much stronger than the one of $n_\rho(\omega)$.

This behavior may be explained by considering the scaling variable $x=\omega b/\gamma v$ which determines the exponential decrease of the impact parameter dependent equivalent photon spectrum. For high equivalent photon

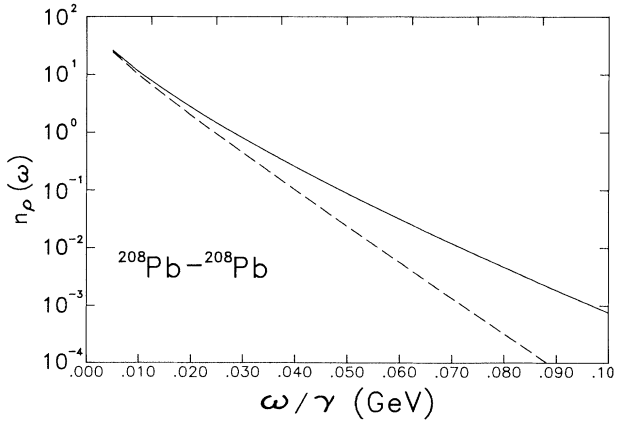

FIG. 4. Impact parameter integrated equivalent photon spectrum as a function of the scaling variable $\tilde{x}=\omega/\gamma$. The solid line corresponds to $n_\rho(\omega)$, while the dashed line corresponds to the usual $n(\omega)$.

energies the main contribution to the integral over the impact parameter dependent spectrum arises from close collisions where the two spectra differ significantly from each other; i.e., the geometrically modified spectrum gives larger contributions. For $n(\omega)$ the exponential decrease is determined by $\omega b/\gamma v > 1$, while for $n_\rho(\omega)$ we mainly have $\omega b'/\gamma v > 1$. While the spectrum $n(\omega)$ is already dominated by the exponentially decreasing parts, $n_\rho(\omega)$ is still not.

The differences of the spectra arise at the high equivalent photon energy part where the overall magnitude is already decreasing exponentially. Effects on the cross sections calculated via Eq. (2.1) are expected to be small if low equivalent photon energies are involved. In the case where only the high-energy tail of the equivalent photon spectrum is tested the use of the geometrically modified equivalent photon spectrum becomes essential for accurate calculations.

The accuracy of the sharp cutoff approximation for $N_\rho(\omega,b)$ [see Eq. (2.24)] is studied in Figs. 5 and 6. There the impact parameter dependent equivalent photon spectrum again is shown as a function of the impact parameter b at fixed $\tilde{x}=\omega/\gamma$. The labeling is the same as in Figs. 2 and 3 except that $N_\rho^{\rm app}(\omega,b)$ is included as the dashed dotted line.

In Fig. 5 we show the spectra at $\omega/\gamma=\frac{30}{100}$ MeV. In this case the approximated spectrum is valid over the whole range considered and practically coincides with the full calculations. Coming back to Eq. (2.25) we find that in this impact parameter region we have

$$x \sim \frac{30\times 50}{100\times 200} \ll 1 \ . \tag{3.3}$$

This provides an excellent approximation of the full spectrum by the approximated one.

In Fig. 6 the same quantity with the same labeling as in Fig. 5 is shown for $\tilde{x}=\frac{500}{100}$ MeV. In this case the validity of the approximation is restricted to 14 fm $\leq b \leq$ 30 fm.

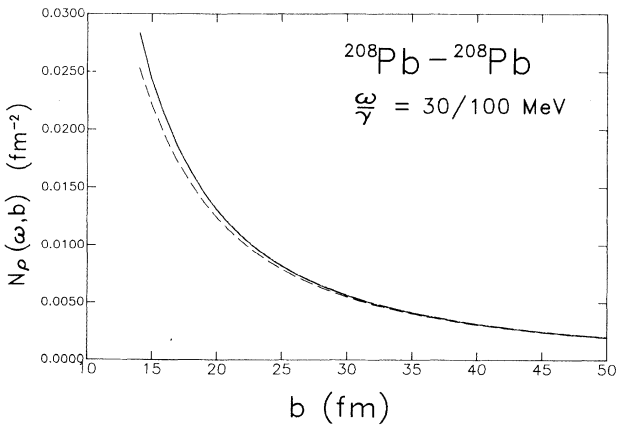

FIG. 5. Same as Fig. 2 for $\tilde{x}=\frac{30}{100}$ MeV. The labeling is also the same as in Fig. 2; the analytic approximation $N_\rho^{\rm app}(\omega,b)$ is added as the dash-dotted line which practically could not be distinguished in this figure from the solid line.

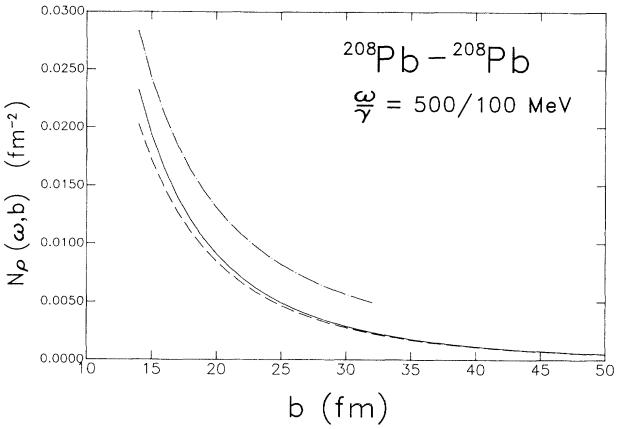

FIG. 6. Same as in Fig. 5 for $\tilde{x}=\frac{500}{100}$ MeV.

The approximation clearly overestimates the full calculation; the corresponding x may be set:

$$x \sim \frac{500\times 15}{100\times 200} \sim O(1) \ . \tag{3.4}$$

If the equivalent photon energy is further increased, the range of validity of the approximation gets smaller; for values of about $\tilde{x}=10$ MeV the approximation Eq. (2.24) completely breaks down.

Since the significant effects of the geometrical modifications of the equivalent photon spectrum on integrated cross sections arise from the region $x \sim 1$, the approximation Eq. (2.24) is not the appropriate one for such calculations. For the calculation of impact parameter dependent cross sections it may be very good, though, special care has to be taken of the corresponding values of x.

B. Luminosity decrease at RHIC and LHC due to electromagnetic fragmentation

During the beam crossing in relativistic heavy ion colliders there will be electromagnetic excitation of the nuclei. Since this excitation leads mainly to particle emission, the electromagnetic interaction contributes to a luminosity decrease. In Ref. [12] the contributions of the giant dipole resonance (GDR) as well as of the e^+e^- pair production with e^- capture were considered. In Refs. [4,5] additionally the contributions of high-energy equivalent photon interactions were taken into account; in Ref. [13] a calculation especially for RHIC conditions has been done using the most accurate experimental data for the photonuclear cross section. In the following we study fragmentation cross sections due to the high-energy photon interactions.

The total cross section for photon-hadron interactions in relativistic heavy ion collisions is given by Eq. (2.1), where $\sigma_{\gamma A}$ is the total cross section for the subprocess γ + nucleus $\rightarrow X$. Above pion threshold this cross section can be approximated by

$$\sigma_{\gamma A}(\omega)=A_{\text{eff}}\left[\frac{Z}{A}\sigma_{\gamma p}(\omega)+\frac{N}{A}\sigma_{\gamma n}(\omega)\right]$$
$$\simeq A_{\text{eff}}\sigma_{\gamma p}(\omega)\ . \tag{3.5}$$

The total cross section (referring to one nucleus) for relativistic heavy ion collisions in this energy region is then given by

$$\sigma_{\text{tot}}=A_{\text{eff}}\int_{\omega_{\text{thres}}}^{\infty}\frac{d\omega}{\omega}n(\omega)\sigma_{\gamma p}(\omega)\ . \tag{3.6}$$

To carry out numerically the integration over ω in Eq. (3.6) we take the experimental values of Refs. [14,15] for the total γ-p cross section. Above photon energies of 4.2 GeV we set $\sigma_{\gamma p}=100$ μb=const over the whole range. As a check we used the analytical approximation given (in units of μb) in Ref. [5],

$$\sigma_{\text{tot}}(>2\text{ GeV})\simeq 0.23A_{\text{eff}}Z^2\ln^2[\omega_{\max}/(2\text{ GeV})]\ , \tag{3.7}$$

where $\omega_{\max}=\gamma_{\text{lab}}\hbar c/2R$ and $\sigma_{\gamma p}=100$ μb is assumed [the corresponding Eq. (2.4) of Ref. [5] refers to the excitation of both nuclei].

The numerical calculation using the conventional equivalent photon spectrum in Eq. (3.6) was compared to Eq. (3.7) and found to be in very good agreement. To study the effect of the geometry we also used the spectrum from Eq. (2.19). The numerical values for the different energy ranges for both calculations are collected in Table I, where the ^{208}Pb-^{208}Pb and the ^{197}Au-^{197}Au system is taken for LHC and RHIC conditions, respectively.

Obviously, the contribution of the high-energy region is large; the contributions from the nucleon resonance region and the asymptotic region (constant $\sigma_{\gamma p}$) are comparable in magnitude. Setting $A_{\text{eff}}=A^{0.9}$, the results for RHIC in Table I (conventional spectrum) are consistent with the calculations of Ref. [13]. In this case we get a 3% enhancement of the cross section in the asymptotic region due to the modification of the equivalent photon spectrum. For this choice of A_{eff} and the asymptotic value of $\sigma_{\gamma p}$ we find a total fragmentation cross section of [taking into account the results for the GDR region from Eq. (2.2) of Ref. [5]]

$$\sigma_{\text{tot}}(\text{LHC})=171\text{ b},\quad \sigma_{\text{tot}}(\text{RHIC})=68\text{ b}\ . \tag{3.8}$$

We want to point out that in Eq. (3.8) the quasideuteron region of the photonuclear cross section is not included. The effect of e^- capture contributes additionally to the luminosity decrease.

The modifications of the total cross section due to the use of Eq. (2.19) for the equivalent photon spectrum are very small. The very-high-energy part of the spectrum contributes only little to the sum in Eq. (3.7); the sum is dominated by the low-energy part of the equivalent photon spectrum.

This can be seen clearly in Figs. 7 and 8. There the corresponding differential cross section $d\sigma_{\text{tot}}/d\sqrt{s}$ is shown as a function of $\sqrt{s}$ in the γN system for RHIC and LHC conditions, respectively. In the RHIC case (Fig. 7) the differential cross section is already exponentially decreasing for energies of $\sqrt{s}>40$ GeV. In this energy region the correct treatment of the geometry in the equivalent photon spectrum via Eq. (2.19) (solid line) in comparison to the conventional method (dashed line) gets essential; the differences are larger than one order of magnitude. In Fig. 8 where the same quantities with the same labeling are shown for LHC conditions, the differences between the methods are negligible up to $\sqrt{s}\sim 700$ GeV. Only above this value do the deviations become relevant. At $\sqrt{s}=210$ GeV, the energy reached in ep collisions at HERA [16], the use of Eq. (2.19) does not lead to any significant changes. In the high-energy region the fragmentation cross section is directly proportional to the elementary γp cross section. The HERA result [16] is given by $154\pm16(\text{stat})\pm32(\text{sys})$ μb at $\sqrt{s}=210$ GeV. The corresponding results in Table I therefore can easily be scaled with any preferred value of the γp cross section. The argument may be turned around by making use of the extremely hard part of the

TABLE I. Total photonuclear cross section integrated over the indicated equivalent photon energy range for ^{208}Pb-^{208}Pb and ^{197}Au-^{197}Au collisions at LHC and RHIC conditions, respectively. The GDR region can be taken from Ref. [5].

LHC: ^{208}Pb-^{208}Pb	0.17–2 GeV	2–10 GeV	>10 GeV
$\frac{1}{A_{\text{eff}}}\sigma_{\text{tot}}$ (mb)	237.36	63.91	157.60
$\frac{1}{A_{\text{eff}}}\sigma^{\rho}_{\text{tot}}$ (mb)	238.42	64.20	159.44
$A_{\text{eff}}=A^{0.9}$: σ_{tot} (b)	28.95	7.80	19.22
RHIC: ^{197}Au-^{197}Au			
$\frac{1}{A_{\text{eff}}}\sigma_{\text{tot}}$ (mb)	50.48	10.46	6.94
$\frac{1}{A_{\text{eff}}}\sigma^{\rho}_{\text{tot}}$ (mb)	50.93	10.62	7.22
$A_{\text{eff}}=A^{0.9}$: σ_{tot} (b)	5.86	1.21	2.23

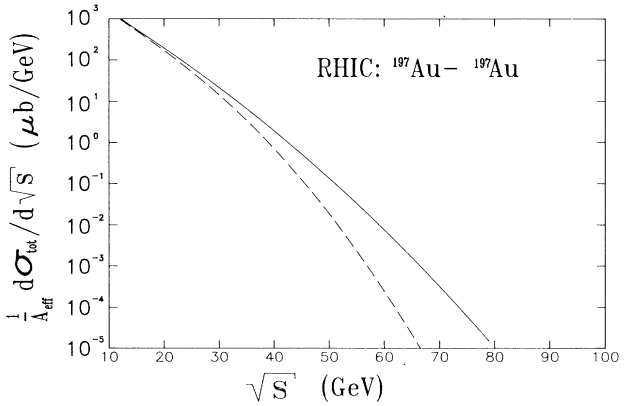

FIG. 7. Differential cross section $d\sigma_{\text{tot}}/d\sqrt{s}$ divided by A_{eff} as a function of $\sqrt{s}$ of the γp system for RHIC conditions in ^{197}Au-^{197}Au collisions. For the asymptotic value of $\sigma_{\gamma p}$ we set $\sigma_{\gamma p}=100$ μb. The solid line corresponds to the calculation using $n_{\rho}(\omega)$, while the dashed line corresponds to the use of the conventional $n(\omega)$.

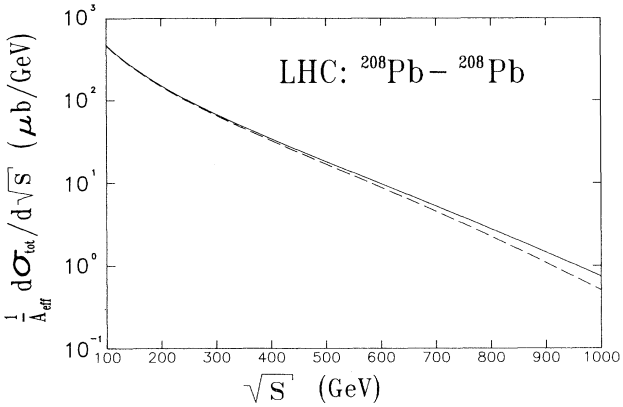

FIG. 8. Same quantity as in Fig. 7 with the same labeling for LHC conditions in ^{208}Pb-^{208}Pb collisions.

equivalent photon spectrum in ultrarelativistic heavy ion collisions to measure the γN cross section in this energy region.

The improved treatment of the equivalent photon spectrum due to the geometry of the system is of minor importance for the total cross sections. This is due to the fact that the deviations from the conventional method become important only in the very-high-energy range where the overall contribution to the total cross section is very small.

IV. PHOTON-GLUON FUSION IN RELATIVISTIC HEAVY ION COLLISIONS

The determination of the distribution functions of partons in hadrons is essential to investigate the structure of hadrons, to test QCD in general as well as to understand the physics at present and future hadron colliders. In measurements of deep inelastic scattering processes with lepton beams the quark and sea quark distribution functions have been investigated. The determination of the gluon distribution function is of special interest since, for example, it is well known that the gluons carry about 50% of the momentum of the proton. So far, the gluon distribution function is only known to some extent, i.e., for values of x essentially above 0.1. Since these experiments are not directly sensitive to the gluon distribution function, the determination proceeds mainly indirect through the determination of the proton structure functions [17]. However, there are processes such as the photoproduction of heavy quarks which are directly sensitive to the gluon distribution function. There are first measurements of the charm production at Fermilab [18] and also at HERA there are plans to measure charm production for the determination of the gluon distribution function [19]. In peripheral collisions at 100 GeV/nucleon (RHIC) and 3400 GeV/nucleon (LHC) where the direct strong interactions are completely suppressed, there is a large flux of high-energy equivalent photons. Apart from other reactions, this flux leads to heavy quark production via $\gamma\gamma$ and γg fusion. Because of the small electromagnetic coupling the heavy quark production in such collisions is dominated by the γg fusion. The possible determination of the gluon distribution function in such experiments was proposed and studied theoretically in Ref. [6].

The elementary subprocess of the γg fusion was studied theoretically starting in the 1970's (see Refs. [20–22]). The equivalent photon method is a powerful tool for the treatment of photon induced reactions in peripheral ultrarelativistic heavy ion collisions (see, e.g., [2]). The basic relation for the calculation of the heavy quark production cross section in peripheral ultrarelativistic heavy ion collisions is given by

$$d\sigma_{q\bar{q}} = 2\frac{n(\omega)}{\omega} G_g(x) d\sigma_{\gamma g \to q\bar{q}}(\hat{s}) d\omega\, dx \ , \tag{4.1}$$

where $\hat{s}$ is determined in the γg subsystem and x is the Bjorken scaling variable. The gluon distribution function is denoted by G_g, while $n(\omega)$ is the equivalent photon spectrum. In the high-energy limit the Bjorken scaling variable is given by

$$x = \frac{\hat{s}}{s} \ , \tag{4.2}$$

where s refers to the γN subsystem.

Assuming that $d\sigma_{\gamma g \to q\bar{q}}$ for the production of heavy quarks is known accurately, the correct deduction of the gluon distribution function $G_g(x)$ from Eq. (4.1) requires a proper knowledge of the equivalent photon spectrum. Calculations using the conventional spectrum $n(\omega)$ were already done in Ref. [6]. In the following we want to apply the improved equivalent photon spectrum Eq. (2.19) and compare the results to calculations where the conventional spectrum $n(\omega)$ is used.

In principle, Eq. (4.1) contains the gluon distribution function of the whole nucleus under consideration. Since we want to point out mainly the modifications due to the treatment of equivalent photon spectrum, we set

$$G_g(x,Q^2) = A_{\text{eff}} G_N(x,Q^2) \ . \tag{4.3}$$

Shadowing (antishadowing) effects (see, e.g., Ref. [23]) or nuclear modifications such as the gluonic European Muon Collaboration effect (Refs. [24,25] and references quoted therein) are not explicitly included in our approach. Phenomenologically, we use an effective nucleon number in Eq. (4.3); this is also done in Ref. [6]. For the gluon distribution function $G_N(x,Q^2)$ we take the fit of Ref. [26] at $Q_0^2 = 4(\text{GeV}/c)^2$. To test the sensitivity on the gluon distribution function also slightly different types are tested [6].

For integrated cross sections we may simply rewrite Eq. (4.1) in terms of the invariant mass of the produced $q\bar{q}$ pair $M_{q\bar{q}}$, leading to

$$\frac{1}{A_{\text{eff}}} \frac{d\sigma_{q\bar{q}}}{dM_{q\bar{q}}} = 4M_{q\bar{q}} \sigma_{\gamma g \to q\bar{q}}(M_{q\bar{q}}^2) \times \int_{M_{q\bar{q}}^2}^{\infty} \frac{ds}{s^2} G_N\left[\frac{M_{q\bar{q}}^2}{s}\right] n_{(\rho)}(s) \ . \tag{4.4}$$

The notation $n_{(\rho)}$ indicates that calculations are per-

formed either with the conventional equivalent photon spectrum or with the geometrically modified spectrum Eq. (2.19). The total elementary $\gamma g \to q\bar{q}$ cross section is given in lowest order by (see, e.g., Ref. [27])

$$\sigma_{\gamma g \to q\bar{q}}(\hat{s}) = \frac{2\pi\alpha\alpha_s e_q^2}{2\hat{s}} \left[(3-\beta^4) \ln\left[\frac{1+\beta}{1-\beta}\right] - 2\beta(2-\beta^2) \right], \quad (4.5)$$

where we defined $\beta = \sqrt{1-m_q^2/\hat{s}}$. The strong coupling is denoted by α_s and e_q is the charge of the quark in units of the electron charge. The range of validity of Eq. (4.5) is restricted to $\hat{s} = M_{q\bar{q}}^2 > 4m_q^2$, which is the production threshold for the $q\bar{q}$ pair. We use the running coupling constant α_s evaluated at m_q^2 (see, e.g., Refs. [20,6]):

$$\alpha_s = \frac{12\pi}{(33-2n_f)\ln(m_q^2/\Lambda^2)}, \quad (4.6)$$

where n_f is the number of flavors ($n_f = 4$) and $\Lambda = 0.4$ GeV [26,27].

We want to point out that in Eq. (4.4) the integration contains both the equivalent photon spectrum and the gluon distribution function. The gluon distribution function enters over the whole range of the Bjorken variable x; Eq. (4.4) may only be used to get information on the product of the distributions. To be directly sensitive to the gluon distribution function, especially to obtain transparent information on the small x region we may also rewrite Eq. (4.1) in terms of $\sqrt{s}$ of the γN system:

$$\frac{1}{A_{\text{eff}}} \frac{d\sigma_{q\bar{q}}}{d\sqrt{s}} = \frac{2n_{(\rho)}(\sqrt{s})}{\sqrt{s}} \int_{4m_{q\bar{q}}^2}^{s} d\hat{s}\, G_N\left[\frac{\hat{s}}{s}\right] \sigma_{\gamma g \to q\bar{q}}(\hat{s}) . \quad (4.7)$$

In Eq. (4.7) the gluon distribution function enters for a fixed value of $\sqrt{s}$ only down to a value of $x_{\min} = 4m_{q\bar{q}}^2/s$.

In the following we restrict ourselves to ^{208}Pb-^{208}Pb and ^{197}Au-^{197}Au collisions at LHC and RHIC conditions, respectively. Our calculations are performed for $c\bar{c}$ production, where we use $m_c = 1.74$ GeV [18]. In Figs. 9 and 10 the differential cross section $d\sigma_{c\bar{c}}/dM_{c\bar{c}}$ divided by the effective nucleon number A_{eff} is shown as a function of the invariant mass $M_{c\bar{c}}$ of the $c\bar{c}$ system for LHC and RHIC conditions, respectively. The solid line corresponds to Eq. (4.4) using the geometrically modified equivalent photon spectrum Eq. (2.19), while for the dashed one the conventional spectrum has been used. In Fig. 9 (LHC conditions) the energy scale where the deviations between the two calculations become significant is well above invariant masses of 500 GeV. For invariant masses of about 1000 GeV, where the cross section is dominated by the exponential decrease of the equivalent photon spectra, the deviations are about one order of magnitude. In Fig. 10 (RHIC conditions) the energy scale is shifted corresponding to the characteristic Lorentz factor. At invariant masses of about 15 GeV the geometrically modified calculation (solid line) gives

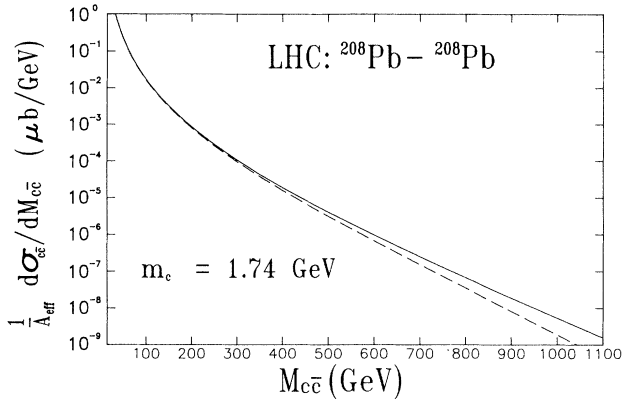

FIG. 9. Differential cross section $d\sigma_{c\bar{c}}/dM_{c\bar{c}}$ divided by A_{eff} as a function of the invariant mass $M_{c\bar{c}}$ of the $c\bar{c}$ pair is shown for ^{208}Pb-^{208}Pb collisions at LHC conditions. The solid line corresponds to Eq. (4.4) with the use of the geometrically modified equivalent photon spectrum; the dashed one corresponds to the use of the conventional spectrum. For the charm quark mass we use $m_c = 1.74$ GeV [18].

significantly larger cross sections; the difference is of one order of magnitude if invariant masses of 30 GeV and larger are reached.

The same comparison but in terms of $\sqrt{s}$ in the γN system is shown in Figs. 11 and 12 for LHC and RHIC conditions, respectively. In Fig. 11 the differential cross section $d\sigma_{c\bar{c}}/d\sqrt{s}$ from Eq. (4.7) divided by the effective nucleon number A_{eff} is shown as a function of $\sqrt{s}$ (same labeling as in Figs. 9 and 10) for LHC conditions. For energies above 700 GeV the differences become significant, reaching one order of magnitude above 1400 GeV. For energies of about 700 GeV the gluon distribution function is tested down to values of $x = 2.5 \times 10^{-5}$, which is well below the region open to HERA [19]. In Fig. 12, where the same quantities as in Fig. 11 are shown, the energy scale is again correspondingly shifted. Clear differences in the two calculations arise at 20 GeV; the cross section using the conventional equivalent pho-

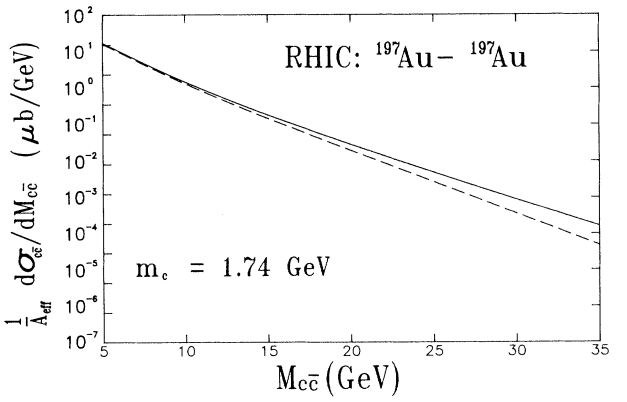

FIG. 10. Same as in Fig. 9 but for ^{197}Au-^{197}Au collisions at RHIC conditions (also same labeling).

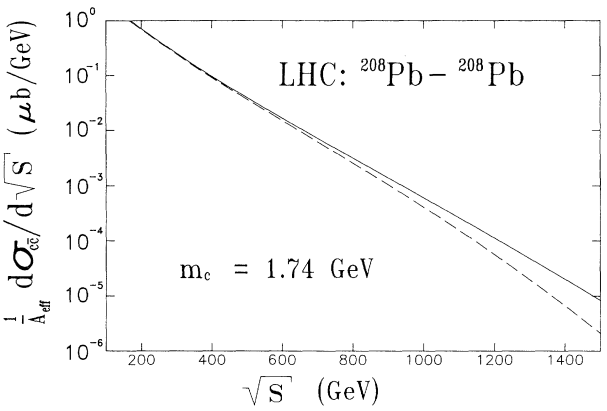

FIG. 11. Differential cross section $d\sigma_{c\bar{c}}/d\sqrt{s}$ divided by A_{eff} as a function of $\sqrt{s}$ in the γN system is shown for ^{208}Pb-^{208}Pb collisions at LHC conditions. The labeling of the lines and the choice of the charm quark mass are the same as in Fig. 9.

ton spectrum decreases much more strongly than the one corresponding to the geometrically modified spectrum. For energies of about 30 GeV at RHIC values of $x=0.01$ are reached.

The procedure of reconstructing the invariant mass $M_{c\bar{c}}$ or $\sqrt{s}$ from the experiments is described in Ref. [19]. The consideration of the $\sqrt{s}$ spectra (see Figs. 11 and 12) seems to be advantageous since it gives more insight into the characteristics of the gluon distribution function. According to Eq. (4.7) the gluon distribution function is only folded with the elementary cross section and tested down to small values of x. The equivalent photon spectrum enters directly into the calculation; therefore, the importance of the use of the geometrically modified spectrum is directly determined by the spectrum (see Fig. 4). The invariant mass spectrum (Figs. 9 and 10) is less sensitive to the use of the geometrically modified equivalent photon spectrum. This originates from the fact that in Eq. (4.4) there is a folding of the two distribution functions and the elementary cross section; the contributions of the high-energy tail of the equivalent photon spectra to the integral in Eq. (4.4) are suppressed. The correct use of the geometrically modified equivalent photon spectrum becomes important in the high-energy region. For RHIC conditions at an energy scale of about 20 GeV this is essential for the possible determination of the gluon distribution function, while the corresponding energy scale for LHC conditions is at around 700 GeV.

To get greater insight into the possibility of determining the gluon distribution function from Eq. (4.4) or (4.7), the sensitivity to different choices for this function has to be studied. We use the following gluon distribution functions [$Q_0^2=4$ (GeV)/$c)^2$], also used in Ref. [6]:

$$xG(x)=0.879(1+9x)(1-x)^4 , \tag{4.8a}$$

$$xG(x)=1.564(1+9x)(1-x)^6 , \tag{4.8b}$$

$$xG(x)=0.22x^{-0.8}(1-x)^6 , \tag{4.8c}$$

$$xG(x)=0.79x^{-0.5}(1-x)^5 . \tag{4.8d}$$

In Eqs. (4.8a)–(4.8d), x is the Bjorken scaling variable. So far, Eq. (4.8a) has been used.

In Fig. 13 the same quantities as in Fig. 11 are shown for the four different gluon distribution functions [$(1/A_{\text{eff}})d\sigma_{c\bar{c}}/d\sqrt{s}$ as a function of $\sqrt{s}$]. Label 1 corresponds to the use of Eq. (4.8a), 2 to the use of Eq. (4.8b), 3 to the use of Eq. (4.8c), and 4 to the use of Eq. (4.8d). The solid lines correspond to the use of the geometrically modified equivalent photon spectrum in Eq. (4.7), while the dashed lines correspond to the use of the conventional spectrum in Eq. (4.7). For energies below 600 GeV the cross sections are well separated, independent of the use of the modified equivalent photon spectrum or the conventional one. In this energy region the differences due to the different gluon distribution functions are large. Above 800 GeV the differences due to the different gluon distribution functions are of the order of the ones due to the different equivalent photon spectra (see labels 1 and 2, labels 3 and 4). In this energy region the use of the

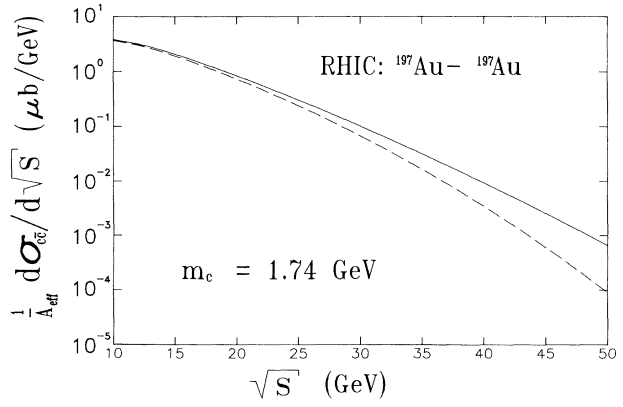

FIG. 12. Same as in Fig. 11 but for ^{197}Au-^{197}Au collisions at RHIC conditions (also same labeling).

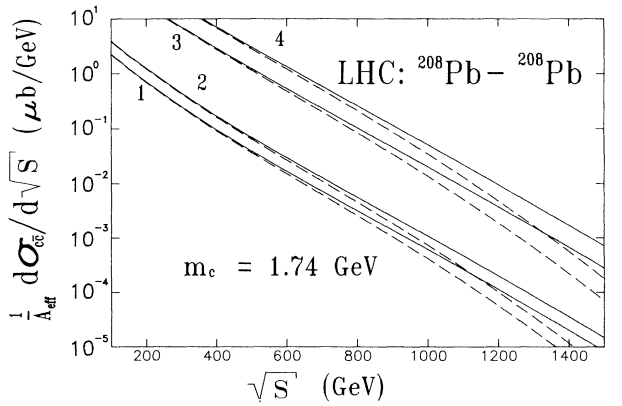

FIG. 13. Same as in Fig. 11 for the four different gluon distribution functions labeled by 1–4. Label 1 corresponds to Eq. (4.8a), label 2 to Eq. (4.8b), label 3 to Eq. (4.8c), and label 4 to Eq. (4.8d).

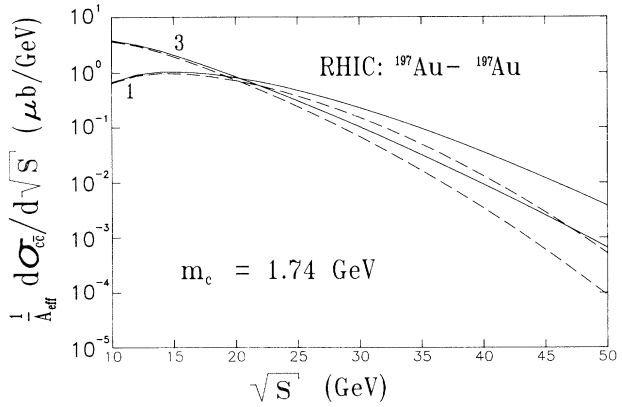

FIG. 14. Same as in Fig. 13 but for ^{197}Au-^{197}Au collisions at RHIC conditions (only labels 1 and 3 are shown).

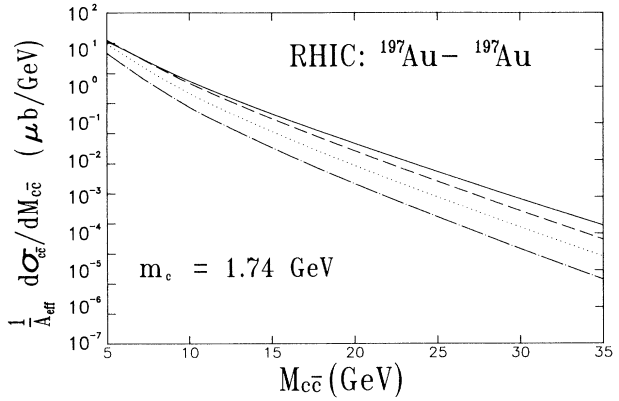

FIG. 16. Same as in Fig. 15 but for ^{197}Au-^{197}Au collisions at RHIC conditions (also same labeling).

geometrically improved equivalent photon spectrum is essential for the proper separation of the different types of gluon distribution functions.

In Fig. 14 the same quantities with the same labeling as in Fig. 13 are shown for ^{197}Au-^{197}Au collisions at RHIC conditions. For reasons of clearness only labels 1 and 3 are shown. In the RHIC case also for low energies it is essential to use the geometrically modified equivalent photon spectrum to determine properly the gluon distribution function.

In Figs. 15 and 16 the effect of varying the gluon distribution function is studied for $d\sigma_{c\bar{c}}/dM_{c\bar{c}}$ as a function of $M_{c\bar{c}}$. In these figures we only show the calculations using the geometrically modified equivalent photon spectrum. The solid line corresponds to the gluon distribution function Eq. (4.8a), the dashed one to Eq. (4.8b), the dash-dotted one to Eq. (4.8c) and the dotted one to Eq. (4.8d). In Fig. 15 the calculations for ^{208}Pb-^{208}Pb collisions at LHC conditions are shown. The differences between the lines corresponding to the different gluon distribution functions are less pronounced in comparison to the $\sqrt{s}$ spectra. Above 500 GeV the different gluon distribution functions lead to significant variations in the differential cross section. In Fig. 16 the same quantities with the same labeling are shown for ^{197}Au-^{197}Au collisions at RHIC conditions. Significant differences due to the gluon distribution functions are obtained over a wide range of invariant masses $M_{c\bar{c}}$ (already above 10 GeV).

The cross sections $d\sigma_{c\bar{c}}/d\sqrt{s}$ and $d\sigma_{c\bar{c}}/dM_{c\bar{c}}$ for $c\bar{c}$ production in peripheral relativistic heavy ion collisions via γg fusion are sensitive to the use of the equivalent photon spectrum. For high energies the use of the geometrically modified equivalent photon spectrum is important for a proper description; especially for RHIC conditions, this is essential. For the determination of the gluon distribution function from such processes the study of $d\sigma_{c\bar{c}}/d\sqrt{s}$ is most suitable; the sensitivity leads to significant differences over a wide range of energies. For this purpose the correct input for the equivalent photon spectrum, especially for RHIC conditions, is also essential.

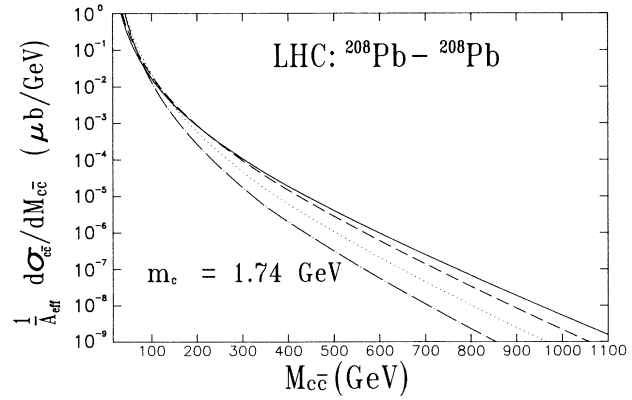

FIG. 15. Same as in Fig. 9 for the four different gluon distribution functions. The solid line corresponds to the use of Eq. (4.8a), the dashed one to Eq. (4.8b), the dash-dotted one to Eq. (4.8c), and the dotted one to Eq. (4.8d).

V. CONCLUSIONS

In close peripheral relativistic heavy ion collisions at RHIC and LHC conditions there are copious (equivalent) photon-hadron interactions at very high photon energies. Because of the strong impact parameter dependence of the equivalent photon spectrum in such collisions we explicitly take into account the finite spatial distribution of constituents in the nucleus struck by the equivalent photon. We apply the impulse approximation and derive explicitly a geometrically modified impact parameter dependent equivalent photon spectrum. An analytical approximation of this geometrically modified spectrum is also obtained. The modifications in the impact parameter dependent spectrum are significant for small impact parameters; for very large impact parameters the modified spectrum coincides with the conventional one. For the impact parameter integrated spectra the geometrical modifications lead to an enhancement of the high-energy tail. The use of scaling variables leads to a transparent

presentation.

In the framework of the equivalent photon method total fragmentation cross sections contributing to the luminosity decrease at RHIC and LHC conditions are studied including the geometrically modified equivalent photon spectrum. The contribution of the nucleon resonance region and of the asymptotic region are comparable in magnitude. The effect of including the geometrical modifications of the equivalent photon spectrum is of minor influence. For ^{208}Pb-^{208}Pb collisions at LHC conditions a total fragmentation cross section of $\sigma_{\text{tot}}=171$ b, for ^{197}Au-^{197}Au collisions at RHIC conditions $\sigma_{\text{tot}}=68$ b is obtained (excluding the quasideuteron contribution).

In distant heavy ion collisions it may be possible to determine the gluon distribution function from the heavy $q\bar{q}$ production via the γg fusion process [6]. In the framework of the equivalent photon approximation the cross sections are given by folding the equivalent photon spectrum and the gluon distribution function with the elementary $q\bar{q}$ production cross section. For charm quark production the differential cross sections $d\sigma_{c\bar{c}}/d\sqrt{s}$ and $d\sigma_{c\bar{c}}/dM_{c\bar{c}}$ indicate the importance of the use of the geometrically modified equivalent photon spectrum in the high-energy region. Especially for RHIC conditions this is essential. To show the sensitivity of the cross sections on the gluon distribution function several parametrizations are tested explicitly. For RHIC as well as for LHC conditions the variation due to the different gluon distribution functions is of the same order of magnitude as the differences due to the use of the geometrically modified equivalent photon spectrum in contrast to the conventional one. Especially for RHIC conditions it is essential to use the correct input for the equivalent photon spectrum to get a proper signature for the gluon distribution function.

Photon-hadron interactions at very high photon energies in relativistic heavy ion collisions depend sensitively on the input of the equivalent photon spectrum. In general, the use of the geometrically modified spectrum for such reactions is of special importance.

The process of heavy $q\bar{q}$ production via the γq fusion is of further special interest. Therefore a more extensive study on the angular distributions of the corresponding two jet events in the framework of the equivalent photon approximation should be done in the future.

ACKNOWLEDGMENTS

One of the authors (N.B.) would like to thank the Studienstiftung des deutschen Volkes for the support of his studies. Stimulating discussions with Professor G. Soff and M. Vidovic are gratefully acknowledged.

[1] M. L. Goldberger and K. M. Watson, *Collision Theory* (Wiley, New York, 1964).
[2] C. A. Bertulani and G. Baur, Phys. Rep. **163**, 299 (1988).
[3] G. Baur, IKP Annual Report, Forschungszentrum Jülich, ISSN 0366-0885, 1992, p. 155; G. Baur and N. Baron, contribution to Quark Matter 93, Borlänge, Sweden, 1992 (unpublished).
[4] D. Brandt, Report No. SPS/AMS/Note/89-6, 1989; (private communication).
[5] G. Baur and C. A. Bertulani, Nucl. Phys. **A505**, 835 (1989).
[6] Ch. Hofmann, G. Soff, A. Schäfer, and W. Greiner, Phys. Lett. B **262**, 210 (1991).
[7] J. D. Jackson, *Classical Electrodynamics* (Wiley, New York, 1975).
[8] G. Baur and L. G. Ferreira Filho, Phys. Lett. B **254**, 30 (1991).
[9] A. I. Akhiezer and V. B. Berestetskii, *Quantum Electrodynamics* (Interscience, New York, 1965).
[10] G. Baur and N. Baron, Nucl. Phys. **A561**, 629 (1993).
[11] I. S. Gradstein and I. M. Ryshik, *Tafeln-Tables* (Deutsch, Frankfurt, 1981).
[12] Conceptual Design of the Relativistic Heavy Ion Collider RHIC, Report No. BNL52195, 1989, p. 119.
[13] M. J. Rhoades-Brown and J. Weneser, AD/RHIC-110, Informal Report No. BNL-47806, 1992.
[14] T. A. Armstrong *et al.*, Phys. Rev. D **5**, 1620 (1972).
[15] F. A. Berends and A. Donnachie, Nucl. Phys. **B84**, 342 (1975).
[16] ZEUS Collaboration, Phys. Lett. B **293**, 465 (1992).
[17] CDHSW Collaboration, P. Berge *et al.*, Z. Phys. C **49**, 187 (1991).
[18] J. C. Anjos *et al.*, Phys. Rev. Lett. **65**, 2503 (1990).
[19] R. van Woudenberg *et al.*, in Proceedings of the DESY Workshop Physics at HERA, Hamburg, FRG, 1991, Report No. DESY 92-002, FTUAM EP-92-01, 1992.
[20] H. Fritzsch and K.-H. Streng, Phys. Lett. **72B**, 385 (1978).
[21] M. Glück and E. Reya, Phys. Lett. **79B**, 453 (1978).
[22] L. M. Jones and H. W. Wyld, Phys. Rev. D **17**, 759 (1978).
[23] P. Casterina and A. Donnachie, Z. Phys. C **49**, 481 (1991).
[24] EM Collaboration, J. J. Aubert *et al.*, Phys. Lett. **123B**, 275 (1983); E. L. Berger and F. Coester, Annu. Rev. Nucl. Part. Sci. **37**, 463 (1987).
[25] S. Kumano, Phys. Lett. B **298**, 171 (1993).
[26] D. W. Duke and J. F. Owens, Phys. Rev. D **30**, 49 (1984).
[27] F. Halzen and A. D. Martin, *Quarks & Leptons: An Introductory Course in Modern Particle Physics* (Wiley, New York, 1984).